# A coherent structure based approach to modeling wall-turbulence

Dennice F. Gayme and Benjamin A. Minnick

*Johns Hopkins University*

(Dated: February 27, 2020)

## Abstract

Coherent structures in the form of streamwise elongated streaks and vortices play a key role in energy growth, momentum transfer and the self-sustaining processes underlying wall-bounded turbulent flow. A wide range of conceptual and physics based models have been employed to analyze the role of these structures. This article focuses on the restricted nonlinear (RNL) modeling framework, a physics based approach that simplifies the flow representation, based on the dominance of streamwise coherent structures. This model is formed by decomposing the Navier-Stokes (NS) equations into a streamwise constant (averaged) mean flow and perturbations about that mean. Order reduction is then obtained through a dynamical restriction of the nonlinear interactions between the perturbations. We review the success of this model in reproducing statistical and spectral properties of wall-bounded turbulent flows at moderate Reynolds numbers and within a large-eddy simulation (LES) framework in the limit of infinite Reynolds number. An analysis of energy transfer in half-channel RNL flow highlights the critical non-linearity and scale interactions necessary to sustain turbulence at moderate Reynolds numbers. Our results also indicate that the fundamental properties of wall-bounded turbulence such as skin friction drag are robust to dynamical restrictions of streamwise-varying interactions, which may lend to the difficulty in controlling these flows. The article concludes with a discussion of ongoing challenges for the RNL model and the need to unify existing approaches to meet the challenges of characterizing and controlling high-Reynolds number wall-turbulence.

## INTRODUCTION

Characterizations of wall-bounded turbulent flows in terms of coherent motions (structures) has propelled fundamental advances in our understanding of these flows. The identification of velocity streaks and vortical structures through visualization techniques [1, 2] and statistical correlations [3, 4] led to our early understanding of the structure of turbulent boundary layers [1, 5]. The associated descriptions of the flow interactions in the near-wall region laid the foundation for the well-accepted conceptual model of the near-wall cycle [6] that drives a self-sustaining process (SSP) in the near-wall region [7–13]. This work has also informed our understanding of the energy transfer (production and dissipation) near the wall, e.g. [14, 15], which is fundamental to the friction drag that has long been the target of flow control efforts.

Streamwise coherent structures, referred to as large [16–18] and very large-scale coherent motions (streaks) [19, 20], have also been observed in the core region of a wide range of wall-bounded turbulent flows. The significance of these types of structures away from the wall has been demonstrated through a number of studies detailing their significant contributions to the Reynolds stresses and turbulent transport processes throughout the flow [19, 21–24], particularly at high Reynolds numbers. The wall normal extent of these large-scale structures leads to an influence near the wall that includes the provision of a significant contribution to the local kinetic energy [19, 22] as well as modulation of the near-wall structures [23, 25].

The influence of the large-scale structures near the wall is consistent with the attached eddy hypothesis [5]. This hypothesis and subsequent refinements to the attached eddy model [26–29] form, perhaps, the most widely used conceptual model of wall-bounded turbulence. It is built upon the notion of organized hierarchies of self-similar eddies (i.e., coherent structures) that grow with distance from the wall. Although the model relies on coherent structures, only aspect ratios of these eddies are prescribed. The predictive capabilities of the attached eddy hypothesis with respect to the turbulence statistics have made it a powerful tool in evaluating candidate structures observed in experiments such as the low momentum zones forming inside vortex packets [23]. The existence of self-similar structures that scale with distance from the wall arising from this theory has also formed the basis of recent works that have identified and characterized a family of self-sustaining processes at a range of flow scales [30–32].

The eddies in the attached eddy hypothesis have recently been related to invariant solutions of the Navier-Stokes (NS) equations [33]. These invariant solutions, first identified by Nagata [34], take the form of three-dimensional equilibria (fixed points), traveling wave solutions, or periodic orbits of the NS equations, see e.g. [35–41]. Their resemblance to the coherent structures (streaks and vortices) observed in canonical flows has led to their being called exact coherent structures [38] and their description in terms of vortex-wave interactions in the asymptotic high Reynolds number limit [13, 42, 43]. Kawahara *et al.* [44] provides a full discussion of these solutions and the dynamical systems viewpoint that seeks to build a skeleton of turbulence through the continuations of the unstable manifolds providing pathways between them. A complete characterization of the relationship between these structures and fully developed turbulence is a topic of ongoing work, see e.g. [43–49].

The discussion above highlights a subset of the approaches that have exploited the notion of coherent motions to advance our understanding of wall-turbulence; a more comprehensive discussion of coherent structure based analysis of wall-turbulence can be found in the recent reviews [50–52] and references therein. These approaches have informed recent developments in linear and nonlinear representations of wall-turbulence based on simplifications of the NS equations. This article focuses on one such representation, the restricted nonlinear (RNL) model [53–56]. Its underlying assumption that the large-scales of the flow field are dominated by streamwise coherent motion is based on the importance of these structures in the dynamics of near-wall [10–12] and large-scale motions [19, 21, 24]. The RNL model is derived through a dynamical restriction of the NS equations, which is obtained by first partitioning the dynamics of the flow field into a streamwise constant (averaged) mean flow and a streamwise-varying perturbation field (where perturbations are defined about that mean) and then neglecting or parametrizing the nonlinear interactions between the perturbations [53, 57][58]. The RNL system thus maintains the nonlinear flow physics that lead to momentum transfer [59, 60] and the associated increased shear stress at the wall that is characteristic of wall-turbulence, but the dynamical restriction makes it more computationally and analytically tractable than the NS equations.

The remainder of this article is organized as follows. The next section reviews studies of the linearized NS (LNS) equations and highlights their role in motivating the RNL modeling paradigm. We then describe the RNL system within the context of the wider class of quasi-linear (QL) models that it falls within. This is followed by a review of results that

highlight the ability of RNL simulations to predict statistical quantities, structural features and the transport of energy within a turbulent channel flow. An restricted nonlinear large eddy simulation (RNL-LES) model is used to demonstrate that the RNL dynamics in the infinite Reynolds number limit reproduce log-law behavior across a range of grid sizes. We conclude with a discussion of next steps and continuing challenges for models of wall-bounded turbulence.

## THE LINEARIZED NAVIER STOKES EQUATIONS

Linearizations of the NS equations are perhaps the most widely used mathematical approximation of the dynamics of wall-bounded shear flows. Studies of this dynamical system have been influential in characterizing the importance of coherent structures, and in particular identifying the types of structures that contribute to energy growth. For example, analysis of these equations in transitioning flows demonstrated that initial conditions showing the largest energy growth were coherent structures in the form of streamwise vortices and streamwise coherent streaks [61–64]. Similar structures arise from investigations based on the pseudo-spectrum of the generator of the LNS equations [65]. Linear analysis in the fully turbulent regime employing linearizations about a turbulent mean profile also identified near-wall and outer-layer streamwise streaks as the two types of perturbations sustaining the maximum energy growth [66–69]. The spanwise extents of the identified structures were consistent with structures observed in channel and boundary layer flows. These results are consistent with related studies showing that streamwise vortices and streaks maintain the largest steady-state variance due to spatio-temporal delta-correlated (Gaussian) forcing of the NS equations linearized about both laminar and turbulent mean velocity profiles [69, 70].

Jovanović and Bamieh [71] adopted a systems theoretic view to further analyze the structure arising from the LNS equations. They considered an input-output response wherein the input to the system of equations (in this case, stochastic delta-correlated body forcing) results in a forced response (output), typically the velocity field. Such a viewpoint emphasizes energy amplification i.e. "the ratio of output energy (e.g. steady state variance of the velocity perturbations) to that of the input" [72], rather than the growth of an initial perturbation. This amplification can quantified through the spatio-temporal frequency response (transfer function) of the LNS equations with an external excitation, $\mathcal{H}(k_x, k_z, \omega)$, where

$(k_x, k_z)$ are the streamwise, spanwise wave-numbers and $\omega$ is the temporal frequency [73]. Explicitly, given an external forcing $d(x, y, z, t)$, with Fourier transform $\hat{d}(y; k_x, k_z, \omega)$ the associated spatio-temporal Fourier transform of the velocity field in the streamwise $(x)$, spanwise $(z)$ directions and time can be obtained through the transfer function relationship

$$\hat{\mathbf{u}}(y; , k_x, k_z, \omega) = \mathcal{H}(k_x, k_z, \omega)\hat{d}(y; k_x, k_z, \omega). \tag{1}$$

The transfer function, $\mathcal{H}(k_x, k_z, \omega)$, can be used to characterize a number of the flow properties in terms of different norms of this three dimensional operator [71]. One important example is the squared $H_2$ norm

$$\|\mathcal{H}\|_2^2(k_x, k_z) = \frac{1}{2\pi}\int_{-\infty}^{\infty} trace\{\mathcal{H}(k_x, k_z, \omega)\mathcal{H}^*(k_x, k_z, \omega)\}\, d\omega, \tag{2}$$

where we have omitted the dependence on $y$ for notational convenience. With the appropriate output operator this squared norm can be used to compute the scale-dependent steady-state variance (turbulent kinetic energy) due to delta-correlated (to the size of the spatial filter) stochastic excitation. Jovanović and Bamieh [74] used this interpretation to characterize the dominant energy pathways in channel flow, demonstrating that cross-plane body forcing leads to far greater energy growth, scaling with the Reynolds number cubed, $Re^3$, versus forcing of the streamwise velocity components which leads to linear scaling with Reynolds number. These authors further showed that streamwise constant structures show the largest input-output amplification, exceeding that of structures related to the Tollmien-Schlichting modes that become unstable above a critical Reynolds number [75].

Resolvent analysis is similarly based on the spatio-temporal frequency response of the linear part of the evolution equations for fluctuations about a turbulent (time-averaged) mean but differs in the interpretation of the nonlinear terms in the NS equations as an intrinsic forcing rather than an external excitation, see e.g. [50, 76, 77]. In this way, the forced system is precisely the full NS equations for the fluctuating quantities. The linear transfer function or resolvent operator can then be analyzed in isolation, which is of interest because linear mechanisms are believed to be responsible for energy extraction from the mean, i.e. the nonlinearity is thought to be passive, see e.g. [78]. The framework also lends itself to the study of the resolvent operator response due to triadically consistent nonlinear forcing functions. This formalism has been widely used to study coherent structures in wall-bounded turbulence, see e.g. [50, 77, 79] and references therein. The energetic dominance of

the leading singular values of the resolvent operator (transfer function), has been exploited to identify low order representations of turbulent wall-bounded flows in terms of the leading (highest energy) response modes [79–81]. These modes have been shown to correspond to important flow structures such as the streamwise streaks discussed previously. Superposition of these modes has also been used to construct packets of hairpin vortices [77]. The singular functions of the resolvent operator have been shown to exhibit geometric self-similarity [80] consistent with that observed in previous studies of the LNS equations [69]. Insights regarding observed amplitude modulation of small-scale structures [25] by the outer flow have also been gained by looking at particular triadic interactions [79]. Nonlinear interactions between resolvent modes constrained by the self-similar structures have been investigated to provide analyze the scaling of turbulent fluctuations in the log-layer [82].

Linear models have the benefit of analytical tractability, and as discussed above, have proven invaluable in the study of wall-turbulence. However, turbulence is an inherently nonlinear phenomena, and as such finding a reduced order representation of the key nonlinear interactions is expected to produce new insights into wall-bounded turbulence. The conceptual model of the nonlinearity as an intrinsic forcing in the resolvent analysis framework can be regarded as a bridge between the LNS and nonlinear representations of turbulence. The next section describes a more direct reduced order nonlinear model for wall-bounded turbulence whose underlying assumptions are informed by the results of the linear analysis highlighted in this section. In particular, the importance of the streamwise coherent structures in the growth and amplification of energy in wall-bounded shear flows along with the ability of low order approximations to capture key features of turbulence as formalized in studies of the stochastically forced LNS [70] and the resolvent framework [79–81].

## THE RESTRICTED NONLINEAR MODELING PARADIGM

Approximating the NS equations through a dynamical restriction of the nonlinear interactions provides a simplified system based on the flow physics that can preserve important nonlinear interactions while reducing the analytical and computational burden associated with analyzing the full NS equations. One method of forming such an approximation is to view the flow as having a large-scale or 'mean' governed by a nonlinear evolution that is dynamically coupled to a linear perturbation field that can be used to construct the covari-

ance of the flow. The dynamical restriction takes the form of limiting nonlinear interactions between perturbations to those that contribute directly to the predefined large-scale, with others either parameterized or neglected.

One approach to forming such models is through statistical state dynamics or cumulant expansions [57, 83–86] comprised of evolution equations for the mean (large-scale) and its covariance. The higher order cumulants are typically either parameterized as stochastic forcing or set to zero. These models offer analytical tractability that has been exploited to understand mechanisms underlying wall-bounded turbulence, see e.g. [56, 57, 87, 88]. However, the need to directly simulate the evolution of the covariance leads to computational challenges due to its $\mathcal{O}(N^2)$ growth with grid size $N$.

QL models also form a large-scale using a spectral cut-off, typically as a horizontal average (i.e. $k_x = k_z = 0$ in Fourier space). However, in contrast to the statistical state dynamics approach, the evolution of the perturbations about the mean (small-scales) are approximated through linear dynamics that neglect or parameterize nonlinear interactions between perturbations, i.e. interactions between $k_x \neq 0$ and $k_z \neq 0$ Fourier modes that do not contribute to the mean (add to zero). Nonlinear interactions between the mean and the perturbations and those contributing to the mean (large-scale) flow couple the mean and perturbation dynamics. The QL model has been widely applied to problems in atmospheric sciences, where it has been shown to accurately predict statistical quantities in baroclinic turbulence and atmospheric boundary layers, see e.g., [86, 89, 90]. As the separation of scales increases or the dynamics become more complex, the accuracy of the QL model can be improved through a generalized quasi-linear (GQL) model that alters the spectral cut-off for the large-scale mean to include $k_x, k_z > 0$ Fourier modes [91]. This change in spectral cut-off corresponds to permitting nonlinear interactions between a subset of the non-zero streamwise and spanwise modes. The GQL model thus transfers energy across a wider range of flow scales, which improves the accuracy of the statistics. GQL models have been successfully applied to investigate zonal jets [91], helical magneto-rotational instability [92], and rotating Couette flow [93].

The RNL model of wall-bounded turbulent flows can be interpreted as either a QL model with a two-dimensional mean flow or a GQL model with streamwise wave-number cutoff of $k_x = 0$ and a spanwise wave-number cutoff corresponding to the size of the spatial filter. However, it differs in the definition of the perturbation field, which is typically constrained to

a fixed set of streamwise varying modes. The equations are formed by first decomposing the total velocity field, $\mathbf{u}_T(x,y,z,t) = (u_T, v_T, w_T)$ into a streamwise constant mean, $\mathbf{U}(y,z,t) = (U,V,W) = \langle \mathbf{u}_T \rangle_x$, and perturbations about this mean, $\mathbf{u}(x,y,z,t)$. Here the coordinates $(x,y,z)$ denote the streamwise, wall-normal, and spanwise directions respectively. The angle brackets with subscript $x$ denote streamwise-averaging, i.e. $\langle \phi \rangle_x = \frac{1}{L_x} \int_0^{L_x} \phi \, dx$ for flow variable $\phi$; which is represented by the $k_x = 0$ mode in a Fourier representation. Here $L_x$ denotes the streamwise extent of the domain; the wall-normal and spanwise domain lengths are respectively denoted by $\delta$ and $L_z$. The nonlinear interactions between the perturbations, $\mathbf{u} \cdot \nabla \mathbf{u} - \langle \mathbf{u} \cdot \nabla \mathbf{u} \rangle_x$ are then neglected to obtain

$$\partial_t \mathbf{U} + \mathbf{U} \cdot \nabla \mathbf{U} + \nabla P/\rho - \nu \nabla^2 \mathbf{U} = -\langle \mathbf{u} \cdot \nabla \mathbf{u} \rangle_x, \tag{3a}$$

$$\partial_t \mathbf{u} + \mathbf{U} \cdot \nabla \mathbf{u} + \mathbf{u} \cdot \nabla \mathbf{U} + \nabla p/\rho - \nu \nabla^2 \mathbf{u} = 0, \tag{3b}$$

and $\nabla \cdot \mathbf{u}_T = 0$. The RNL system thus comprises the dynamics of a large-scale streamwise constant mean flow field (represented in Fourier space as $k_x = 0$) driven by a streamwise varying ($k_x \neq 0$) perturbation field, as depicted in figure 1. These perturbations, whose nonlinear interactions are restricted to non-zero wave-numbers such that $k_{x,m} + k_{x,n} = 0$, are treated as small-scales that are regulated by the mean flow. Conceptually the large-scale here represents the evolution of the streamwise elongated coherent structures, (streaks, rolls and vortices discussed above), while the perturbation field represents the small-scale turbulence interacting with these coherent motions.

This notion that streamwise constant dynamics form an appropriate representation of the large-scales is supported by the observed prevalence and importance of these structures [16–24] in wall-turbulence as well as their role in the energy amplification observed in studies of the LNS [61–70, 74, 75]. In addition, streamwise constant nonlinear interactions have been shown to reproduce the mean momentum transfer associated with shape of the turbulent velocity profile in canonical flows, [59, 60, 94, 95]. Simulations of stochastically forced streamwise constant dynamics, in which the right hand side in (3a) is replaced by stochastic excitation that is delta-correlated in space and time, of both Couette flow [94] and pipe flow [95] led to 'turbulent-like' flows that reproduce the shape of the mean velocity profile along with other important structural features of the flow. These computational studies coupled with the analysis in [60, 94] provide evidence that this choice indeed captures key large-scale flow phenomena.

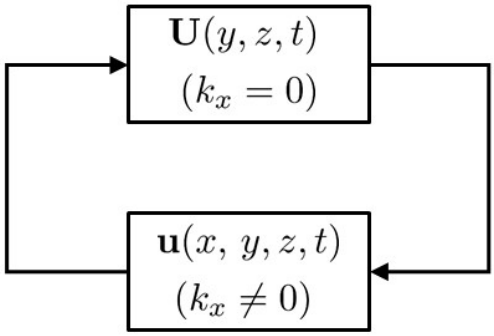


FIG. 1: Schematic illustrating the coupling between the streamwise constant mean (top block) whose evolution (3a) is driven by the streamwise constant ($k_x = 0$) part of the $\langle \mathbf{u} \cdot \nabla \mathbf{u} \rangle_x$ of the nonlinear interactions between streamwise varying perturbations (bottom block). The dynamics of the perturbations are in turn regulated through nonlinear interactions with the mean flow; which are captured through the term $(\mathbf{U} \cdot \nabla \mathbf{u} + \mathbf{u} \cdot \nabla \mathbf{U})$ in (3b).

The coupled dynamics of the RNL model (see figure 1) overcomes the requirement of persistent forcing to maintain the turbulent state that is inherent in streamwise constant models, whose laminar states in plane Couette and pipe flow are known to be globally asymptotically stable [96, 97]. The accuracy of the self-sustaining RNL turbulence attained through simulations of the coupled model was shown to reproduce accurate low-order statistics and roll/streak structures in low Reynolds number plane Couette flow at vastly reduced computational expense [53, 98]. In fact, one of the major advantages of the RNL model is that it can accurately reproduce these critical flow features in plane Couette and channel flows when the perturbation field is restricted to as few as one streamwise varying modes interacting with the mean flow [98, 99]. However, the choice of these modes, which we refer to as the streamwise wave-number support, greatly affects the accuracy of the RNL flow field [55, 56, 99].

There is strong evidence that the streamwise wave-number support that leads to RNL dynamics that correctly reproduce the momentum transfer, low order statistics and energy transport at low to moderate Reynolds numbers corresponds to the peak of the pre-multiplied surrogate dissipation spectra in the outer-layer [100]. This quantity is computed as

$$\nu k_x (E_{\omega_x \omega_x}(k_x, y) + E_{\omega_y \omega_y}(k_x, y) + E_{\omega_z \omega_z}(k_x, y)), \tag{4}$$

where the streamwise vorticity spectra is given by, $E_{\omega_x\omega_x}(k_x, y) = \langle\overline{\hat{\omega}'_{T_x}\hat{\omega}'^{*}_{T_x}}\rangle_z$ [101]. The symbol $\hat{\phi}$ signifies the streamwise Fourier transform of the flow variable $\phi$, the angle brackets with subscript $z$ indicates spanwise-averaging, i.e. $\langle\phi\rangle_z = \frac{1}{L_z}\int_0^{L_z}\phi\ dz$ and the over-bar denotes time-averaging. The prime ($'$) indicates the fluctuation from this average, i.e., $\phi'_T = \phi_T - \overline{\phi_T}$. The respective wall-normal and spanwise vorticity spectra, $E_{\omega_y\omega_y}(k_x, y)$ and $E_{\omega_z\omega_z}(k_x, y)$, are computed similarly using the respective components of the total vorticity vector $\boldsymbol{\omega}_T := [\omega_{T_x}, \omega_{T_y}, \omega_{T_z}]^T$, where the superscript $()^{\mathbf{T}}$ denotes the transpose. The surrogate dissipation differs from the true dissipation in that it neglects the cross velocity gradients, i.e., it represents the approximation $\varepsilon = \nu\overline{\boldsymbol{\omega}'_T \cdot \boldsymbol{\omega}'_T} + 2\nu\overline{[(\nabla\mathbf{u}_T)' : (\nabla\mathbf{u}_T)'^{\mathbf{T}}]} \approx \nu\overline{\boldsymbol{\omega}'_T \cdot \boldsymbol{\omega}'_T}$, where (:) indicates an inner product of two second-order tensors. These neglected terms provide a small contribution to the overall dissipation in channel flow, particularly in the region away from that wall that is of interest here [102]. In this work, we follow the convention of [101] and normalize this surrogate dissipation spectra by its maximum value at each $y^+$.

Figure 2 shows the $k_x$ pre-multiplied surrogate dissipation spectra (4) normalized by its maximum value at each $y^+$ for the Reynolds numbers considered by Bretheim *et al.* [99]. In that work, the single wave-number support with the best fit to the skin-friction coefficient of DNS data at the corresponding Reynolds number was empirically computed based on a number of RNL simulations with different streamwise wave-number support. Figure 3 shows the resulting 'optimal' wavelengths as a function of $Re_\tau$, plotted alongside the resulting mean velocity profiles for all of the Reynolds numbers that they considered. The 'optimal' wavelengths found in Bretheim *et al.* [99], shown in figure 3, are superimposed onto the plots in figure 2 as vertical dashed lines. These plots demonstrate a clear correspondence between the 'optimal' wave-number support of the RNL dynamics at each Reynolds number and the outer-layer peak of the surrogate dissipation spectra. This agreement suggests that these most dissipative streamwise structures in the outer-layer provide the parametrization of the RNL dynamics necessary to capture the correct momentum transfer in this low to moderate Reynolds number range.

The results in figure 3(b) indicate that the 'optimal' wavelength of RNL turbulence tends to a constant value as the Reynolds number is increased [99]. This behavior is consistent with that of the peak range for the outer-layer surrogate dissipation spectra, whose peak of $\lambda_x^+ \approx 150$ illustrated for $Re_\tau = 340$ in figure 2 is the same as that seen for data at $Re_\tau = 2000$ in Jiménez [101]. In general, the extent of the streamwise structures responsible

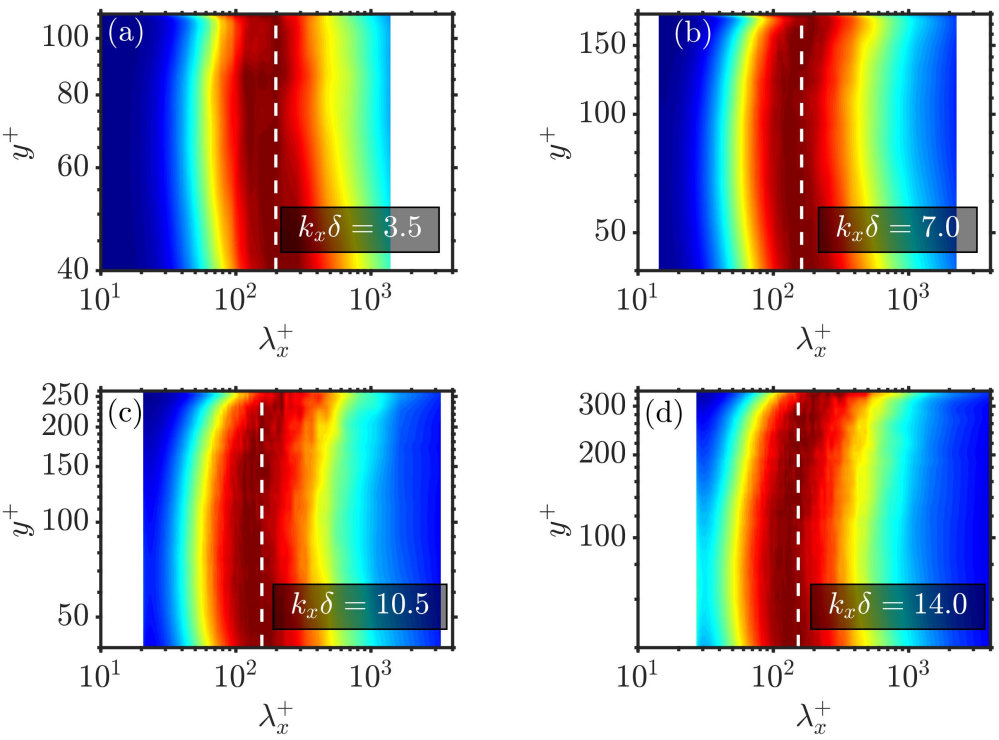


FIG. 2: The peak region of the outer-layer surrogate dissipation spectra from DNS data is shown to coincide with wave-numbers empirically found in Bretheim et al. 2015 [99] for $Re_\tau$: (a) 110, (b) 180, (c) 260, and(d) 340. The spectra is locally normalized by its maximum value at each $y^+$, with color scale from 0 (blue) to 1 (red). The vertical white dashed lines correspond to the 'optimal' streamwise wavelengths shown in figure 3(b).

for the majority of the dissipation in wall-bounded turbulence varies with distance from the wall, with large streaks dissipating most of the energy near the wall. The fact that a single wavelength structure appears to correctly parameterize RNL dynamics in this Reynolds number range is likely due to the fact that the streamwise extent of dissipative structures in the outer-layer does not vary significantly, see figure 2 and figure 1 in [101]. In fact, as shown in [99], including some additional non-zero streamwise wave-numbers to better cover the peak range improves the accuracy of the statistics. Thus, linking the most dissipative outer-layer structures to the correct parametrization of the dynamics, makes the RNL model a predictive reduced order model for wall-bounded turbulent flows across a range of Reynolds numbers.

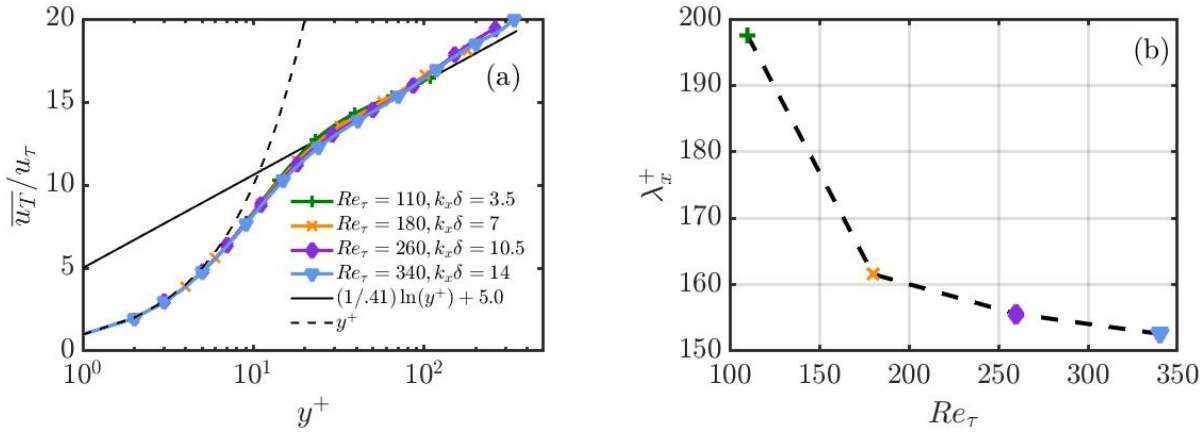


FIG. 3: (a) Mean velocity profiles from simulations of parameterized RNL turbulence at moderate Reynolds numbers predicts log-law behavior. (b) The streamwise wavelengths used in these simulations asymptote to $\lambda_x^+ \approx 150$ as $Re_\tau \to \infty$. Figures adapted from Bretheim *et al.* [99].

## RESTRICTED NONLINEAR DYNAMICS

We now characterize the features of the properly parameterized RNL dynamics across a range of Reynolds numbers. We first illustrate the model's ability to reproduce the key structures associated with the SSP in low Reynolds number plane Couette flow. We then focus on a moderate Reynolds number half-channel flow; first discussing the low-order statistics and pre-multiplied energy spectra. We then examine the extent to which this model, whose parametrization is based on the outer-layer pre-multiplied dissipation spectra, reproduces the transfer of energy near the wall by examining Reynolds stress budgets in the viscous and buffer layers. We end this section with a brief discussion about RNL dynamics at high Reynolds number based on the results from a RNL-LES at effectively infinite Reynolds number, where variations in scale separation are imposed through grid refinement.

### Self-sustaining RNL turbulence

RNL dynamics were first studied in low Reynolds number plane Couette flow [53, 103]. Thomas *et al.* [53, 98] demonstrated that RNL dynamics at $Re_\tau \approx 65$ supported self-sustaining turbulence with accurate low-order statistics. At the Reynolds numbers considered in that work the parametrization based on outer-layer structures is less relevant given

the lack of scale separation in such a flow. Therefore the analysis in this section is based on an unparameterized model, which shows similar statistics to an 'optimally' parameterized model [98].

The RNL turbulence sustained in this low Reynolds number Couette flow was shown to reproduce structural features consistent with the self-sustaining process (SSP), which is fundamental to the maintenance of wall-bounded turbulence. Although the characterization of the mechanisms differ, see e.g. [7, 8, 10, 12, 13, 57, 87, 104], it is well accepted that the SSP comprises an interaction of roll and streak structures. As such, the ability of the RNL model to properly capture this process can be evaluated through an examination of these key structures, which we quantify through the root-mean square (RMS) roll and streak velocities, respectively defined as,

$$\text{RMS Roll Velocity} = \sqrt{\int_0^{L_z} \int_{-\delta}^{\delta} v_T^2 + w_T^2 \; dy \; dz} \tag{5a}$$

$$\text{RMS Streak Velocity} = \sqrt{\int_0^{L_z} \int_{-\delta}^{\delta} (u_T - \langle u_T \rangle_z)^2 \; dy \; dz}, \tag{5b}$$

where as before $\langle \cdot \rangle_z$ denotes the spanwise-averaging operation.

These velocities for an RNL simulation at $Re_\tau = 64.9$ and DNS data at $Re_\tau = 66.2$ are shown in figure 4. Here it is clear that the magnitude and qualitative behavior of both the RMS rolls and streaks are similar in both the DNS and RNL simulations, although the rolls generated by the RNL are somewhat stronger. The results in figure 4 are obtained by forcing both the NS and the RNL dynamics with delta-correlated forcing to initiate the turbulence. This forcing is removed at 500 convective time units, which demonstrates that the rolls and streaks generated through the RNL dynamics are self-sustaining. Further details of the RNL and the associated Stochastic Structural Stability Theory (S3T) SSP can be found in e.g. [53, 56, 57, 87, 98].

**Parameterized RNL turbulence**

We next explore the characteristics of RNL turbulence at the moderate Reynolds number of $Re_\tau = 180$, where scale separation has begun to emerge. We simulate the RNL dynamics using a wave-number support consisting of three non-zero modes, $k_x\delta = 6, 6.5, 7$, that span the peak surrogate dissipation spectra as shown in figure 2(b). This was also the set of

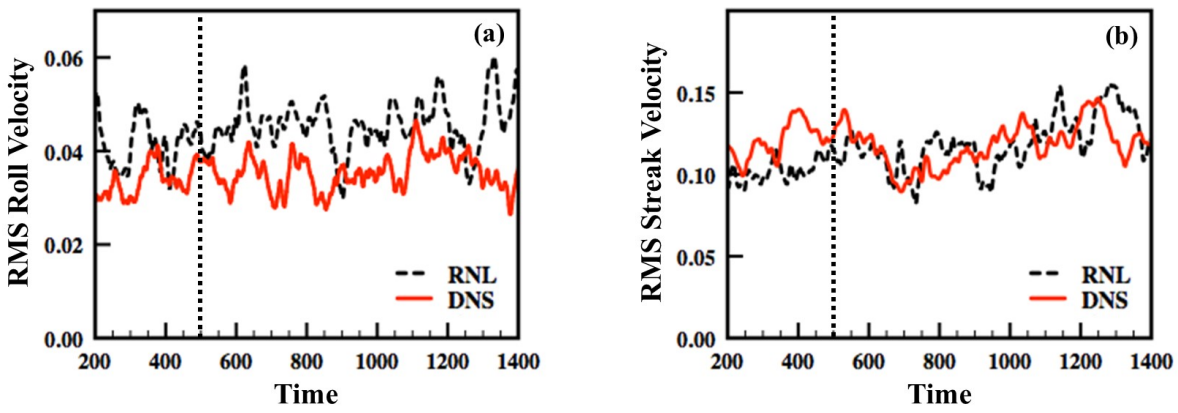


FIG. 4: Root-mean square (a) roll and (b) streak velocities as predicted by DNS (red) and RNL (black dashed). The vertical black dotted line indicates the time when forcing was removed illustrating that RNL self-sustains turbulence similar to DNS. Figures adapted from Thomas *et al.* [53].

modes shown to produce the most accurate mean profile in [99]. The resulting mean velocity, Reynolds stresses, and RMS vorticity fluctuations are plotted in figure 5. Consistent with the results in [99], this parameterized RNL model captures the correct log-law behavior. The Reynolds stresses show good qualitative agreement with DNS and all peak at the correct wall-normal location. The magnitudes of these peaks is however, higher than DNS for the streamwise component of the normal Reynolds stress and lower for both the wall-normal and spanwise components. The agreement of the mean profile and small differences in the Reynolds stresses is remarkable given that the dynamics comprises a two-dimensional mean flow interacting with only three streamwise varying wave-numbers.

The RMS vorticity fluctuations predicted by the parameterized RNL model similarly show good qualitative agreement with the DNS data. More specifically, the parameterized model accurately captures each component of the RMS vorticity beyond $y^+ \approx 60$, but there are small differences in in both the inner- and buffer-layer regions. The spanwise vorticity component ($\omega_{T_z}$), which is dominant, shows higher RMS fluctuations than the DNS data near the wall. This trend reverses in the buffer-layer with the $\omega_{T_z}$ obtained by the RNL simultion taking on lower values than the DNS data. The wall-normal component is more accurate near the wall, but takes on higher values than the DNS data in the buffer-layer. As expected the shape of the streamwise component most closely matches the DNS data,

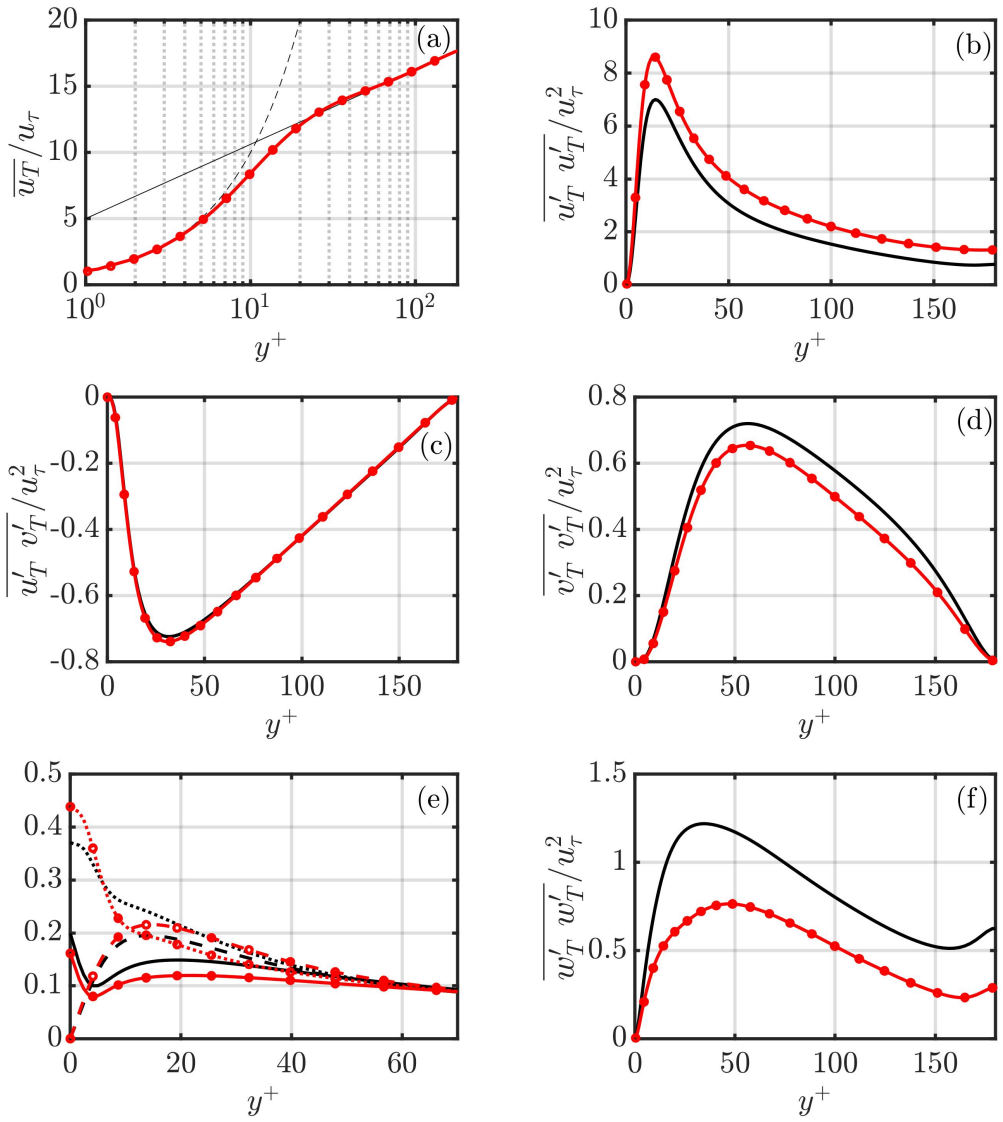


FIG. 5: (a) Mean streamwise velocity from RNL (red circles) and $\overline{u_T}/u_\tau = y^+$ (thin dashed black), $\overline{u_T}/u_\tau = (1/0.41)\ln(y^+) + 5.0$ (thin solid black). (b) Streamwise, (d) wall-normal, (f) spanwise, and (c) cross Reynolds stresses shown with DNS (thick black). (e) Root-mean square (RMS) fluctuations of the streamwise (—), wall-normal (– –), and spanwise ($\cdots$) vorticity.

since the modeling framework emphasizes the cross-plane behavior. This component does however, have the largest quantitative error with the RNL simulation consistently under-predicting its magnitude throughout the near-wall and buffer layers. Although this may seem surprising it is in fact expected as the magnitude of the wall-normal and spanwise velocity fluctuations that comprise this component of vorticity are also under-predicted by

the model, as shown in the wall-normal and spanwise Reynolds stress plots in panels (d) and (f).

The differences in the behavior of the vorticity near the wall are not unexpected as the small scales that dominate the near-wall and buffer-layer vorticity (particularly for the cross-plane components) are under-resolved in the RNL by construction. These results also suggest that parametrization of the model based on the outer-layer surrogate dissipation spectra alters the inner- and buffer-layer dynamics of the parameterized RNL model in order to maintain the correct turbulent mean velocity profile and Reynolds stresses. This idea is further explored in the next subsection.

The differences in the three-dimensional characteristics between RNL turbulence and a turbulent channel flow are illustrated in figures 6(a) and (b), which show a three-dimensional rendering of the total streamwise velocity field. The horizontal planes, taken at $y^+ = 15$, highlight the RNL model's simplified representation of high and low speed streaks elongated in the streamwise direction as a streamwise mean flow interaction with a low dimensional (3 Fourier mode) streamwise varying perturbation field. This figure reflects the inability of the RNL framework to capture streamwise velocity correlations and highlights the limitations of such a quasi-streamwise constant modeling framework. Other quantities that strongly depend on the streamwise variation of the flow field are expected to be similarly poorly resolved. However, figures 6(c) and (d) demonstrate that even with this simplified streak structure, the RNL model captures the cross-plane vortical structures observed in wall-bounded turbulence. This observation is consistent with the accuracy of the RMS streak velocities observed in the low Reynolds number plane Couette flow results in figure 4 and reflects the promise of the RNL model in predicting structures that are important in the SSP as well as in the primary momentum transfer of the flow.

The results in figure 6 point to an important benefit of the RNL framework. The dynamical restriction in the streamwise varying dynamics leads to large computational advantages because only the active streamwise wave-numbers need to be simulated. This is done by computing the nonlinear term as a convolution in $(k_x, y, z, t)$ space instead of as a product in physical space, as is done in DNS. This implementation, which is detailed in [105], eliminates the need to perform transforms back and forth between Fourier and physical space in the streamwise direction to compute the nonlinearity that is typical in pseudo-spectral DNS codes. The reduction in the number of required transforms saves substantial computational

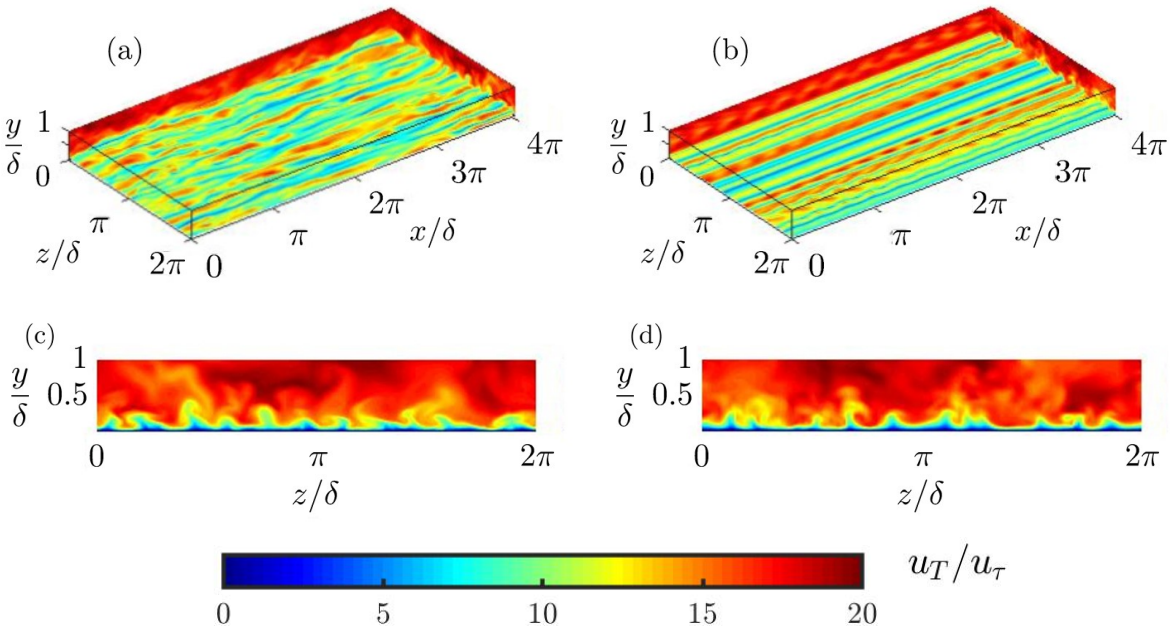


FIG. 6: Snapshots of the instantaneous total streamwise velocity field, $u_T/u_\tau$ from DNS (a and c) and RNL (b and d). The horizontal plane in figures (a) and (b) is at a wall distance of $y^+ = 15$. DNS and RNL simulations show similar spanwise structures in the cross-plane view (c and d)

time and resources over a DNS. For the results presented in this section, the equivalent physical grid for the three non-zero streamwise wave-numbers simulated consists of 8 streamwise grid points. The streamwise grid of the corresponding DNS requires 32× more points for the horizontal resolution considered. This led to the RNL simulations having a measured wall-time speedup of 19.1× given the same hardware. As more streamwise points are needed at higher Reynolds number, we expect this speedup to increase accordingly. A larger speedup could also be achieved with additional optimization of the code. A full characterization of the computational benefits of the RNL framework over a range of Reynolds numbers and streamwise wave-number support sets is a topic of ongoing study.

**Energy spectra and transport in the RNL system**

The parametrization of the RNL model is based on the outer-layer surrogate dissipation spectra. We now explore how constraining the streamwise scales in the RNL dynamics affects the energy spectra and transport of energy in the resulting RNL turbulence.

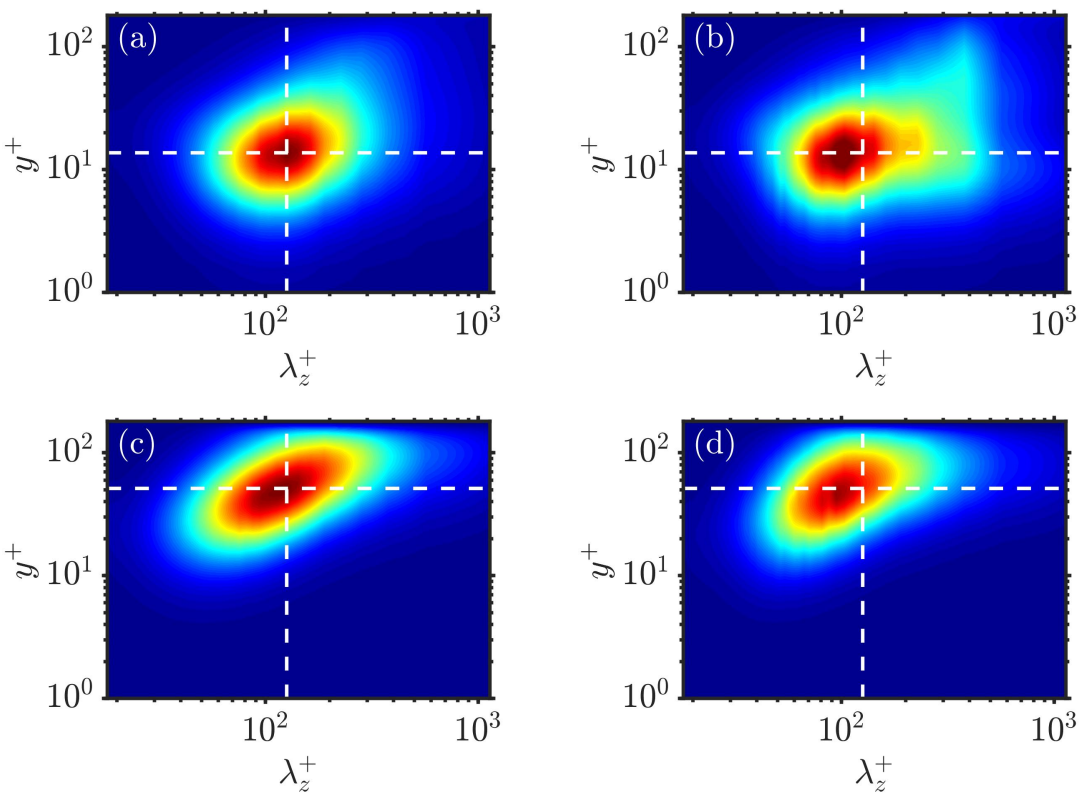


FIG. 7: Pre-multiplied spanwise energy spectra, $k_z E_{uu}$ (a) and (b), and $k_z E_{vv}$ (c) and (d) from DNS (a) and (c) and from RNL (b) and (d). The white dashed lines indicate the wall-normal distance and spanwise wavelengths where the spectra from DNS peaks. These lines are repeated on the spectra predicted from RNL.

Figure 7 shows streamwise and wall normal components of the $k_z$ pre-multiplied one-dimensional energy spectra (respectively $k_z E_{uu}$ and $k_z E_{vv}$) as a function of wall-normal location and spanwise wavelength for DNS data and the $Re_\tau = 180$ RNL simulation described in the previous section. Although these spectra are qualitatively similar, there are some notable differences. The streamwise component of this spectra peaks over a larger range of scales, whereas the wall-normal component of the spectra is more focused. The spanwise wavelength associated with the peak is lower, suggesting that the RNL dynamics introduce additional energy into the small spanwise structures to compensate for the lack of streamwise scales. This small shifting of the energy may account for the ability of the reduced dynamics to so faithfully reproduce the statistical features and energy transfer. Gaining a full understanding this behavior is the focus of ongoing work.

We further analyze the production, dissipation, pressure-strain, and transport rates of

the Reynolds stresses considered in figure 5. The energy budget equation is given by [106]

$$\partial_t R_{ij} + \overline{u_k}\partial_k R_{ij} + \underbrace{\partial_k(\overline{u_i' u_j' u_k'})}_{\text{turbulent transport}} + \underbrace{\partial_k(\overline{p'(u_j'\delta_{ik} + u_i'\delta_{jk})})}_{\text{pressure transport}} - \underbrace{\nu\partial_k\partial_k R_{ij}}_{\text{viscous transport}} =$$
$$\underbrace{2\overline{p's_{ij}'}}_{\text{pressure-strain}} \underbrace{-[R_{ij}\partial_k\overline{u_j} + R_{jk}\partial_k\overline{u_i}]}_{\text{production}} - \underbrace{2\nu\overline{(\partial_k u_i')(\partial_k u_j')}}_{\text{pseudo-dissipation}}, \qquad (6)$$

where we have removed the subscript $T$ for clarity and have adopted index notation with 1, 2, 3 respectively representing the streamwise, wall-normal, spanwise directions. Individual Reynolds stress components are abbreviated as $R_{ij} = \overline{u_i' u_j'}$, the Kronecker-delta symbol is represented as $\delta_{ij}$, and $s_{ij}'$ denotes the time-fluctuating strain-rate tensor. The budgets associated with the streamwise, wall-normal and the cross $R_{12}$ Reynolds stresses are provided in figure 8.

The streamwise component of the normal Reynolds stress, which was higher than that obtained by DNS in figure 5(b), is found to have good agreement throughout the buffer-layer. Here, the RNL production data peaks at the same maximum value and wall-normal location as the DNS data. However the dissipation predicted from the RNL model is slightly lower than DNS, with a higher total transport compensating to obtain the correct energy balance. Increased viscous and turbulent transport rates in the RNL dynamics are responsible for the small differences observed in the streamwise normal Reynolds stress budget. Very near the wall a higher magnitude pseudo-dissipation appears to be balanced by a higher total transport (+ pressure strain). Figure 8(b) indicates that this increase in total transport is due to higher viscous transport in the RNL dynamics.

The wall-normal Reynolds stress, found to be smaller in the RNL dynamics than predicted by DNS in figure 5(d), shows smaller dissipation, transport, and pressure-strain throughout the channel in figure 8. Pressure transport is balanced by pressure-strain near the wall, however smaller maximum values are reached in the RNL dynamics. Further from the wall these terms, and turbulent transport, remain smaller than DNS and reach less pronounced maximum values.

The RNL dynamics predict smaller production and pressure-strain of the cross Reynolds stress away from the wall. Turbulent and pressure transport reach similar values to DNS in this region, however peak further from the wall. Near the wall, pressure-strain and pressure transport balance but maintain higher values in the RNL dynamics than in DNS.

The good agreement of the streamwise component of the normal Reynolds stresses, which

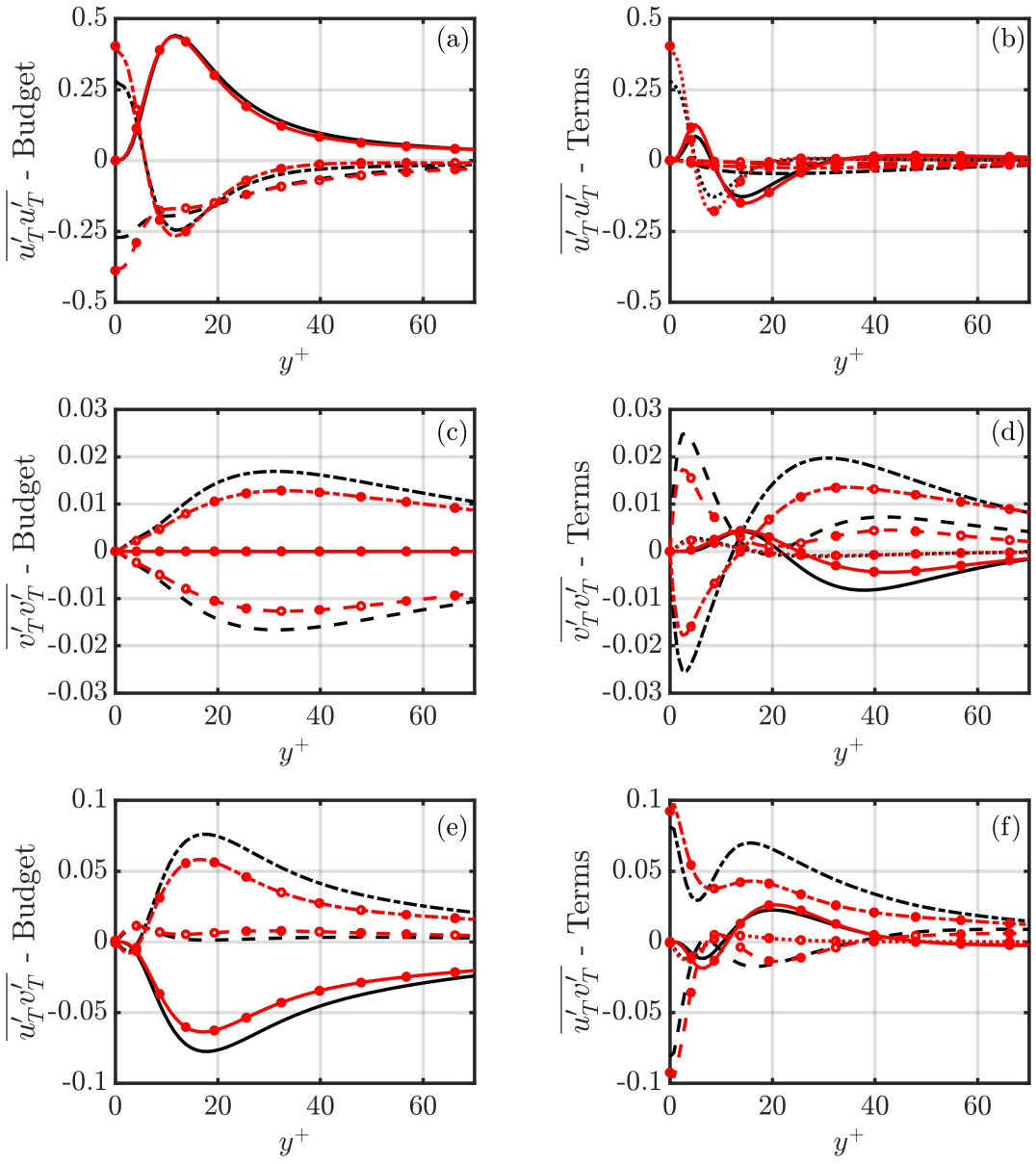


FIG. 8: The streamwise $R_{11} = \overline{u'_T u'_T}$ (a and b), wall-normal $R_{22} = \overline{v'_T v'_T}$ (c and d), and cross $R_{12} = \overline{u'_T v'_T}$ (e and f) Reynolds stress budgets from DNS (black) and RNL (red circles). Figures (a), (c), and (e) include the production (—), dissipation (– –), and total transport + pressure-strain (– -). Figures (b), (d), and (f) show Turbulent transport (—), pressure transport (– –), pressure strain (– -), and viscous transport (· · · ). Markers are sub-sampled for clarity and do not represent grid resolution.

are responsible for the majority of the energy transport is likely responsible for the close agreement between the RNL simulation and DNS data discussed in the previous section.

The relatively smaller in magnitude $R_{22}$ and $R_{12}$ budgets and transport terms show larger differences than the streamwise components $R_{11}$. These trends are consistent with the observations in the second order statistics shown in figure 5, where the lower wall-normal and spanwise Reynolds stresses appear to compensate for the higher streamwise Reynolds stress leading to close agreement in the cross-terms needed to obtain the correct mean velocity profile. A deeper understanding of how the shifts in energy transfer in these terms compensates for the interactions neglected in the RNL to maintain the energy balance of the streamwise components is a topic of continuing work.

**Restricted nonlinear dynamics in the infinite Re limit**

The benefits of a computationally tractable simplified representation of wall-bounded turbulence become increasingly valuable at Reynolds numbers that cannot currently be examined through DNS. In this section, we discuss the potential of the RNL model in predicting the salient characteristics of wall-bounded turbulence at high Reynolds numbers by studying a RNL-LES model. This model, which was introduced in [105] describes filtered velocity and pressure fields, respectively denoted $\tilde{\mathbf{u}}_T(x,y,z,t)$ and $\tilde{p}_T(x,y,z,t)$. As in the derivation of the traditional RNL model, we perform a decomposition into streamwise averaged mean fields, respectively $\tilde{\mathbf{U}}(y,z,t) = \langle \tilde{\mathbf{u}}_T \rangle_x$ and $\tilde{\mathbf{P}}(y,z,t) = \langle \tilde{\mathbf{p}}_T \rangle_x$, along with perturbations about this mean, respectively $\tilde{\mathbf{u}}(x,y,z,t)$ and $\tilde{\mathbf{p}}(x,y,z,t)$. The resulting governing equations are given by

$$\partial_t \tilde{\mathbf{U}} + \tilde{\mathbf{U}} \cdot \nabla \tilde{\mathbf{U}} + \nabla \tilde{P}/\rho - \nu \nabla^2 \tilde{\mathbf{U}} - \nabla \cdot \langle \boldsymbol{\tau}_T \rangle = - \langle \tilde{\mathbf{u}} \cdot \nabla \tilde{\mathbf{u}} \rangle_x \,, \tag{7a}$$

$$\partial_t \tilde{\mathbf{u}} + \tilde{\mathbf{U}} \cdot \nabla \tilde{\mathbf{u}} + \tilde{\mathbf{u}} \cdot \nabla \tilde{\mathbf{U}} + \nabla \tilde{p}/\rho - \nu \nabla^2 \tilde{\mathbf{u}} - \nabla \cdot \boldsymbol{\tau} = 0 \tag{7b}$$

and continuity of the filtered velocity field, $\nabla \cdot \tilde{\mathbf{u}}_T = 0$. The RNL-LES equations only differ from equations (3a) and (3b) by the addition of the streamwise mean and fluctuating parts of the total sub-grid scale stress tensor, $\boldsymbol{\tau}_T$.

The sub-grid scale stress tensor used to model the unresolved scales is approximated by the Smagorinsky model,

$$\boldsymbol{\tau}_T = 2\nu_e \tilde{\mathbf{S}} \quad \text{where} \quad \nu_e = (C_S \Delta)^2 \sqrt{2 \langle \tilde{\mathbf{S}} : \tilde{\mathbf{S}} \rangle_{xz}}. \tag{8}$$

Here, $\Delta$ is the filter width, $\tilde{\mathbf{S}}$ is the filtered strain-rate tensor, and $C_S$ is the Smagorinsky coefficient damped by the Mason wall damping model [105]. The quasi two-dimensional na-

| Label | $N_x = N_z$ | $N_y$ |
|---|---|---|
| L-1 | 64 | 32 |
| L-2 | 128 | 64 |
| L-3 | 192 | 96 |
| L-4 | 256 | 128 |
| L-5 | 384 | 192 |
| L-6 | 512 | 256 |

TABLE I: Grid sizes used in the LES cases in Bretheim *et al.* [105]

ture of the RNL model motivates the use of the horizontally averaged strain-rate magnitude for the eddy viscosity in equation (8). The spanwise and streamwise averaging leads to a one dimensional eddy viscosity $\nu_e$ that provides a similar computational framework to that discussed earlier, i.e. we can simulate in $(k_x, y, z, t)$ space and there is no need for streamwise direction inverse Fourier transformations to the physical space to compute the nonlinearity. We assume an effectively infinite Reynolds number limit ($\nu \to 0$) with a wall-model assuming a roughness height of $y_0/\delta = 1.25 \times 10^{-5}$.

In the RNL-LES paradigm the grid resolution is a proxy for the scale separation induced as Reynolds number increases. This is clear in figure 9, which plots the $k_z$ pre-multiplied spanwise energy spectra, $k_z E_{uu}$, from large eddy simulation (LES) data at a range of grid resolutions (see table I). All cases show a peak that scales with inner units, the spanwise wave-number of which is indicated with a white vertical dashed line. As the grid resolution increases, particularly in cases L-4 to L-6, a second peak scaling with outer units is observed indicating the scale separation expected to be observed as Reynolds number increases.

Bretheim *et al.* [105] demonstrated that the correct parametrization for the RNL-LES dynamics at grid resolutions corresponding to the first four or five grid resolutions (cases L-1–L-5) is based on the $k_x$ pre-multiplied vorticity spectra, which is the appropriate LES analog of the surrogate dissipation spectra. For the rough-wall LES data considered the inner-layer is not resolved, and the streamwise scales associated with the peak show little variation with wall-normal distance, see figure 4 in [105].

The wave-numbers that span the peak range of the vorticity for cases L-1–L-5 are provided in the fourth column of table II. This table also provides the simulation details of the RNL-LES runs in [105]. Figure 10(a) shows that the corresponding mean velocity profiles properly predict log-law behavior for these LES cases. Bretheim *et al.* [105] also demonstrates

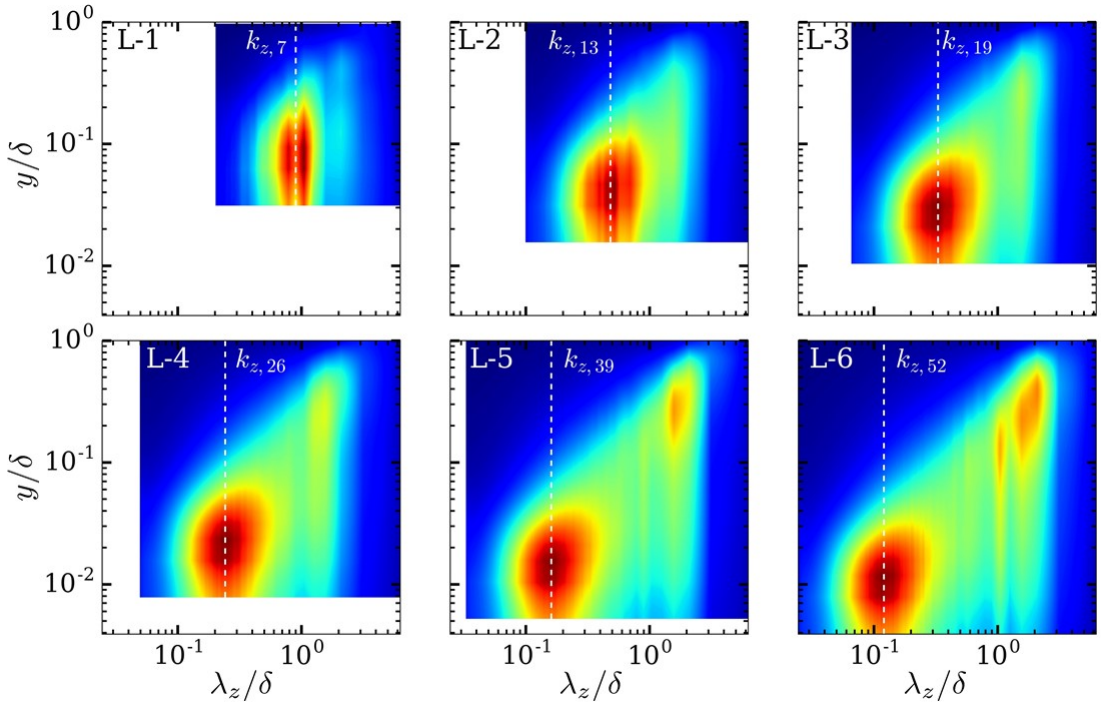


FIG. 9: Pre-multiplied spanwise energy spectra, $k_z E_{uu}$, from LES. The color-bars are the same for each panel, ranging from 0 (blue) to 1 (red). The white vertical dashed lines indicate the spanwise wave-number where the peak is reached. Figure adapted from Bretheim *et al.* [105].

reasonable agreement for the streamwise Reynolds stresses.

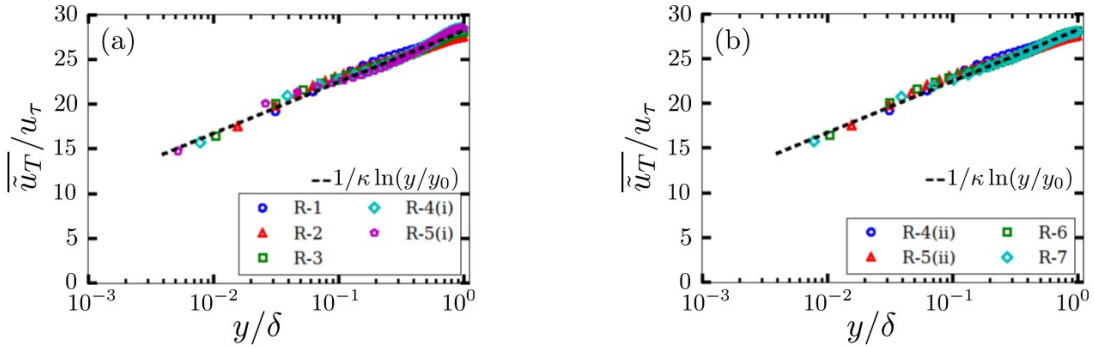


FIG. 10: Mean streamwise velocity from (a) low and (b) high grid-resolution RNL-LES cases. RNL-LES profiles in (b) include the large-scale mode $k_x\delta = 7$. Figure adapted from Bretheim *et al.* [105].

| Label | $N_z$ | $N_y$ | $k_x\delta$ (Regime I) | $k_x\delta$ (Regime II) |
|---|---|---|---|---|
| R-1 | 64 | 32 | 4 | - |
| R-2 | 128 | 64 | 7-9 | - |
| R-3 | 192 | 96 | 10-14 | - |
| R-4(i) | 256 | 128 | 13-18 | - |
| R-4(ii) | 256 | 128 | - | 7,14 |
| R-5(i) | 384 | 192 | 17-25 | - |
| R-5(ii) | 384 | 192 | - | 7, 21 |
| R-6 | 512 | 256 | - | 7, 28 |
| R-7 | 768 | 384 | - | 7,42 |

TABLE II: Cross-plane grid sizes and streamwise wave-numbers for the RNL-LES cases used in Bretheim *et al.* [105]

However, as the grid is refined, the scale separation indicated in figure 9 needs to be captured in the RNL-LES dynamics. This phenomena is accounted for through the addition of a large-scale streamwise wave-number supporting the RNL-LES perturbation field (7b). In particular, Bretheim *et al.* [105] selected $k_x\delta = 7$ which corresponds to $\lambda_x \approx \delta$. Both this large-scale streamwise wave-number and small-scale wave-number corresponding to the peak of the surrogate dissipation spectra from LES are listed under the regime II column of table II. The influence of the large-scale mode was limited near the wall by zeroing out the mode near the wall. This two-band RNL-LES is shown to correctly predict the log-law profile throughout the domain in figure 10(b).

The results in this subsection indicate that a streamwise varying wave-number support for RNL turbulence consisting of a small band (or single) wavelength corresponding to the peak of the surrogate dissipation spectra is unlikely to be sufficient at high Reynolds numbers where scale separation becomes important. The approach in [105] was a preliminary ad-hoc proof of concept. The additional analysis needed to understand how to best introduce additional scales into the RNL perturbation field is an active direction of ongoing research.

## OUTLOOK: ONGOING CHALLENGES FOR WALL-TURBULENCE MODELS

This paper has presented a review of the RNL modeling framework. This modeling paradigm provides a nonlinear but simplified dynamical system that can be used to both analyze and simulate wall-bounded turbulence. Both the fidelity of the results obtained using

an RNL model and the discrepancies provide insight into the dynamics of wall-turbulence. The accuracy of the mean velocity profile obtained in RNL simulations across the range of Reynolds numbers reported indicates that the momentum transfer is indeed dominated by nonlinear interactions between streamwise elongated structures, confirming previous observations in the literature. The ability of the low Reynolds number RNL dynamics with a small-scale perturbation field to self-sustain dynamics that closely resemble wall-bounded turbulence indicates that direct energy transfer from small to large streamwise scales can reproduce the energy transfer necessary to balance production and dissipation across the flow field. This behavior is consistent with the energy cascade being dominated by cross-stream interactions; a notion supported by the shift in the energy spectra to smaller spanwise scales seen in figure 7. The shifting of energy transport to balance dissipation in the energy budgets also provides evidence that the dynamics shift energy as needed to maintain a turbulent state. This ability of the RNL turbulence to compensate for the neglected nonlinear interactions suggests that the SSP underlying wall-turbulence is incredibly robust. The robustness of the turbulent dynamics may explain why control to suppress it presents an ongoing challenge.

The low order representation of the SSP and other key processes offered by the RNL model provide both a computationally and analytically tractable means to not only study the phenomena but to characterize approaches to disrupt the dynamics. This simplified setting has, for example, been exploited to examine the role of the nonlinearity in the maintenance of turbulence and the self-sustaining process, see e.g. [87, 107] in plane Couette flow. RNL models have also been used to study the dynamics of high and low-drag events in turbulent channels [108]. The order reduction obtained through the RNL modeling paradigm has also proven useful in performing parametric studies of flow properties in vertically staggered wind farms [109]. In particular, the RNL-LES model was shown to predict similar power output to a full three-dimensional LES of a wind-farm for some standard vertically staggered configurations. It was then used to evaluate the efficacy of such an approach over a much broader range of parameters that would be accessible with LES [109].

The goal of the RNL paradigm, and in fact, most wall-turbulence models, is a reduction in complexity that facilitates analysis or computational tractability without compromising the ability to reproduce key phenomena. Evaluating the relative benefit of a model, thus requires assessing the extent to which this balance is achieved. Ongoing work further char-

acterizing the RNL model and subsequent extensions of this framework to high Reynolds number regimes is needed to evaluate its inherent trade-offs. This ongoing work will determine the extent of its potential as an analysis and/or predictive tool for closed loop control design in engineering applications. Ultimately, it is unlikely that a single approach will suffice in developing a full understanding of the decades old problem of wall-bounded turbulent flows. Instead the greatest progress is likely to be found by reconciling and combining the different approaches. As previously discussed the attached eddy hypothesis has already been leveraged in resolvent analysis, dynamical systems approaches based on exact coherent structures and a host of other wall-turbulence models. Other work unifying different approaches includes the construction of low dimensional representations of exact coherent structures using resolvent modes [110, 111]. RNL and QL models have also been studied in the context of these invariant solutions to the NS equations [112, 113] with the results of these studies pointing to new directions for modeling efforts. Advancing this already rich set of analysis tools and developing new approaches that draw inspiration from different modeling paradigms may hold the key to characterizing high Reynolds number and non-equilibrium flows.

## ACKNOWLEDGMENTS

The work discussed herein represents the efforts of a number of students, postdoctoral scholars and collaborators. The RNL formulation was developed with Brian F. Farrell and Petros J. Ioannou and the results and discussion herein benefited greatly from long conversations with them. An ongoing collaboration with Charles Meneveau is also gratefully acknowledged as are the contributions of Binh Lieu and Mihailo Jovanović to the early development of the RNL framework and simulation codes. I would also like to note the advancement of the RNL framework by former group members Vaughan Thomas and Joel Bretheim, whose results are highlighted here. We are also thankful for funding support from the NSF and ONR.

[1] S. J. Kline, W. C. Reynolds, F. A. Schraub, and P. W. Runstadler, "The structure of turbulent boundary layers," J. Fluid Mech. **30**, 741–773 (1967).

[2] J. Jeong, F. Hussain, W. Schoppa, and J. Kim, "Coherent structures near the wall in a turbulent channel flow," J. Fluid Mech. **332**, 185214 (1997).

[3] H. P. Bakewell and L. Lumley, "Viscous sublayer and adjacent wall region in turbulent pipe flow," Phys. Fluids **10**, 1880–1889 (1967).

[4] R. F. Blackwelder and R. E. Kaplan, "On the wall structure of the turbulent boundary layer," J. Fluid Mech. **76**, 89–112 (1976).

[5] A. A. Townsend, *The Structure of Turbulent Shear Flow* (Cambridge: Cambridge University Press, 2nd ed., 1976).

[6] F. Waleffe, J. Kim, and J. Hamilton, "On the origin of streaks in turbulent shear flows," in *Eighth Int'l Symposium on Turbulent Shear Flows* (Munich, Germany, 1991).

[7] F. Waleffe, "Hydrodynamic stability and turbulence: Beyond transients to a self-sustaining proccess," Stud. Appl. Math. **95**, 319–343 (1995).

[8] F. Waleffe, "On a self-sustaining process in shear flows," Phys. Fluids A **9**, 883–900 (1997).

[9] F. Waleffe and J. Kim, "How streamwise rolls and streaks self-sustain in a shear flow," in *Self-sustaining mechanisms in wall-bounded turbulence*, edited by R. L. Panton (Computational Mechanics Publications, 1997) pp. 309–332.

[10] K. Hamilton, J. Kim, and F. Waleffe, "Regeneration mechanisms of near-wall turbulence structures," J. Fluid Mech. **287**, 317–348 (1995).

[11] J. Jiménez and A. Pinelli, "The autonomous cycle of near-wall turbulence," J. Fluid Mech. **389**, 335–359 (1999).

[12] W. Schoppa and F. Hussain, "Coherent structure generation in near-wall turbulence," J. Fluid Mech. **453**, 57–108 (2002).

[13] P. Hall and S. Sherwin, "Streamwise vortices in shear flows: Harbingers of transition and the skeleton of coherent structures," J. Fluid Mech. **661**, 178–205 (2010).

[14] P. Orlandi and Javier Jiménez, "On the generation of turbulent wall friction," Phys. Fluids **6**, 634–641 (1994).

[15] J. Kim, S. J. Kline, and W. C. Reynolds, "The production of turbulence near a smooth wall in a turbulent boundary layers," J. Fluid Mech. **50**, 133–160 (1971).

[16] K. J. Kim and R. J Adrian, "Very large scale motion in the outer layer," Phys. Fluids **11**, 417–422 (1999).

[17] C. D. Meinhart and R. J. Adrian, "On the existence of uniform momentum zones in a

turbulent boundary layer," Phys. Fluids **7**, 694–696 (1995).

[18] J. Komminaho, A. Lundbladh, and A. Johansson, "Very large structures in plane turbulent Couette flow," J. Fluid Mech. **320**, 259–285 (1996).

[19] N. Hutchins and I. Marusic, "Evidence of very long meandering features in the logarithmic region of turbulent boundary layers," J. Fluid Mech. **579**, 1–28 (2007).

[20] J. P. Monty, J. A. Stewart, R. C. Williams, and M. S. Chong, "Large-scale features in turbulent pipe and channel flows," J. Fluid Mech. **589**, 147156 (2007).

[21] M. Guala, S. E. Hommema, and R. J. Adrian, "Large-scale and very-large-scale motions in turbulent pipe flow," J. Fluid Mech. **554**, 521–542 (2006).

[22] N. Hutchins and I. Marusic, "Large-scale influences in near-wall turbulence," Phil. Trans. Royal Society of London A **365**, 647–664 (2007).

[23] Ivan Marusic, "On the role of large-scale structures in wall turbulence," Phys. Fluids **13**, 735–743 (2001).

[24] A. J. Smits, B. J. McKeon, and I. Marusic, "High-Reynolds number wall turbulence," Annual Rev. Fluid Mech. **43**, 353–375 (2011).

[25] R. Mathis, N. Hutchins, and I. Marusic, "Large scale amplitude modulation of small-scale structures in turbulent boundary layers," J. Fluid Mech. **628**, 311–337 (2009).

[26] A. E. Perry and M. S. Chong, "On the mechanism of wall turbulence," J. Fluid Mech. **119**, 173–217 (1982).

[27] A. E. Perry, S. M. Henbest, and M. S. Chong, "A theoretical and experimental study of wall turbulence," J. Fluid Mech. **165**, 163–199 (1986).

[28] I. Marusic and J. P. Monty, "Attached eddy model of wall turbulence," Annual Rev. Fluid Mech. **51**, 49–74 (2019).

[29] A. E. Perry and I. Marusic, "A wall-wake model for the turbulence structure of boundary layers. Part 1. Extension of the attached eddy hypothesis," J. Fluid Mech. **298**, 361–388 (1995).

[30] Y. Hwang and C. Cossu, "Self-sustained process at large scales in turbulent channel flow," Phys. Rev. Lett. **105**, 044505 (2010).

[31] Y. Hwang, "Statistical structure of self-sustaining attached eddies in turbulent channel flow," J. Fluid Mech. **767**, 254–289 (2015).

[32] C. Cossu and Y. Hwang, "Self-sustaining processes at all scales in wall-bounded

turbulent shear flows," Philos. Trans. Roy. Soc. London A **375**, 20160088 (2017), https://royalsocietypublishing.org/doi/pdf/10.1098/rsta.2016.0088.

[33] Qiang Yang, Ashley P. Willis, and Yongyun Hwang, "Exact coherent states of attached eddies in channel flow," J. Fluid Mech. **862**, 10291059 (2019).

[34] M. Nagata, "Three-dimensional traveling-wave solutions in plane Couette flow," J. Fluid Mech. **217**, 519–527 (1990).

[35] M. Nagata, "Three-dimensional finite-amplitude solutions in plane Couette flow: bifurcation from infinity," Phys. Rev. E **55**, 2023–2025 (1997).

[36] F. Waleffe, "Three-dimensional coherent states in plane shear flows," Phys. Rev. Lett. **81**, 4140–4143 (1998).

[37] H. Faisst and B. Eckhardt, "Traveling waves in pipe flow," Phys. Rev. Lett. **91**, 224502 (2003).

[38] F. Waleffe, "Exact coherent structures in channel flow," J. Fluid Mech. **435**, 93–102 (2001).

[39] J. Halcrow, J. F. Gibson, P. Cvitanovic, and D. Viswanath, "Heteroclinic connections in plane Couette flow," J. Fluid Mech. **621**, 365–376 (2009).

[40] G. Kawahara and S. Kida, "Periodic motion embedded in plane Couette turbulence: regeneration cycle and burst," J. Fluid Mech. **449**, 291–300 (2001).

[41] S. Toh and T. Itano, "A periodic-like solution in channel flow," J. Fluid Mech. **481**, 67–76 (2003).

[42] P. Hall and F. Smith, "On strongly nonlinear vortex/wave interactions in boundary-layer transition," J. Fluid Mech. **227**, 641–666 (1991).

[43] K. Deguchi and P. Hall, "The high-Reynolds-number asymptotic development of nonlinear equilibrium states in plane Couette flow," J. Fluid Mech. **750**, 99112 (2014).

[44] G. Kawahara, M. Uhlmann, and L. Van Veen, "The significance of simple invariant solutions in turbulent flows," Annual Rev. Fluid Mech. **44**, 203–225 (2012).

[45] J. Jiménez, G Kawahara, M. P. Simens, M. Nagata, and M Shiba, "Characterization of near-wall turbulence in terms of equilibrium and bursting solutions," Phys. Fluids **17**, 015105 (2005).

[46] F. Waleffe, "Exact coherent structures in turbulent shear flows," in *Turbulence and Interactions: Keynote Lectures of the TI 2006 Conference*, edited by Michel Deville, Thien-Hiep Lê, and Pierre Sagaut (Springer Berlin Heidelberg, Berlin, Heidelberg, 2009) pp. 139–158.

[47] J. S. Park and M. D. Graham, "Exact coherent states and connections to turbulent dynamics in minimal channel flow," J. Fluid Mech. **782**, 430–454 (2015).

[48] Subhandu R., C. Cossu, and F. Rincon, "Exact invariant solutions for coherent turbulent motions in Couette and Poiseuille flows," Procedia IUTAM **20**, 94 – 98 (2017), 24th Int'l Congress of Theoretical and Applied Mechanics.

[49] K. Deguchi and P. Hall, "Free-stream coherent structures in parallel boundary-layer flows," J. Fluid Mech. **752**, 602625 (2014).

[50] B. J. McKeon, "The engine behind (wall) turbulence: perspectives on scale interactions," J. Fluid Mech. **817**, P1 (2017).

[51] J. C. Klewicki, G. P. Chini, and J. F. Gibson, "Prospectus: towards the development of high-fidelity models of wall turbulence at large reynolds number," Philos. Trans. Roy. Soc. London A **375**, 20160092 (2017), https://royalsocietypublishing.org/doi/pdf/10.1098/rsta.2016.0092.

[52] J. Jiménez, "Coherent structures in wall-bounded turbulence," J. Fluid Mech. **842**, P1 (2018).

[53] V. Thomas, B. K. Lieu, M. R. Jovanović, B. F. Farrell, P.J. Ioannou, and D. F. Gayme, "Self-sustaining turbulence in a restricted nonlinear model of plane Couette flow," Phys. Fluids **26**, 105112 (2014).

[54] N. C. Constantinou, A. Loranzo-Durán, M-A. Nikolaidis, B. F. Farrell, P. J. Ioannou, and J. Jiménez, "Turbulence in the highly restricted dynamics of a closure at second order: Comparison with DNS," J. Phys.: Conf. Series **506**, 012004 (2014).

[55] B. F. Farrell, P. J. Ioannou, J. Jiménez, N. C. Constantinou, A. Lozano-Durán, and M.-A. Nikolaidis, "A statistical state dynamics-based study of the structure and mechanism of large-scale motions in plane Poiseuille flow," J. Fluid Mech. **809**, 290–315 (2016).

[56] B. F. Farrell, D. F. Gayme, and P. J. Ioannou, "A statistical state dynamics approach to wall turbulence," Philos. Trans. Roy. Soc. London A **375**, 20160081 (2017).

[57] B. F. Farrell and P. J. Ioannou, "Dynamics of streamwise rolls and streaks in wall-bounded shear flow," J. Fluid Mech. **708**, 149–196 (2012).

[58] In practice, this streamwise constant mean is computed as a spatial average.

[59] D. F. Gayme, B. J. McKeon, B. Bamieh, A. Papachristodoulou, and J. C. Doyle, "Amplification and nonlinear mechanisms in plane Couette flow," Phys. Fluids **23**, 065108 (2011).

[60] S.C. Reddy and P.J. Ioannou, "Energy transfer analysis of turbulent plane Couette flow," in *Laminar-Turbulent Transition IUTAM 99*, edited by Saric W. S. and H. F. Fasel (Springer-

Verlag, Berlin, 2000) pp. 211–216.

[61] K. M. Butler and B. F Farrell, "Three-dimensional optimal perturbations in viscous shear flows," Phys. Fluids **4**, 1637–1650 (1992).

[62] S. C. Reddy and D. S. Henningson, "Energy growth in viscous shear flows," J. Fluid Mech. **252**, 209–238 (1993).

[63] B. F. Farrell and P. J. Ioannou, "Perturbation growth in shear flow exhibits universality," Phys. Fluids **5**, 2298–2300 (1993).

[64] L. H. Gustavsson, "Energy growth of three-dimensional disturbances in plane Poiseuille flow," J. Fluid Mech. **224**, 241–260 (1991).

[65] L. N. Trefethen, A. E. Trefethen, S. C. Reddy, and T. A. Driscoll, "Hydrodynamic stability without eigenvalues," Science **261**, 578–584 (1993).

[66] J. C. del Álamo and J. Jiménez, "Linear energy amplification in turbulent channels," J. Fluid Mech. **559**, 205–213 (2006).

[67] C. Cossu, G. Pujals, and S. Depardon, "Optimal transient growth and very-large-scale structures in turbulent boundary layers," J. Fluid Mech. **619**, 79–94 (2009).

[68] G. Pujals, M. García-Villalba, C. Cossu, and S. Depardon, "A note on optimal transient growth in turbulent channel flows," Phys. Fluids **21**, 015109:1–015109:6 (2009).

[69] Y. Hwang and C. Cossu, "Linear non-normal energy amplification of harmonic and stochastic forcing in the turbulent channel flow," J. Fluid Mech. **664**, 51–73 (2010).

[70] B. F. Farrell and P. J. Ioannou, "Stochastic forcing of the linearized Navier-Stokes equations," Phys. Fluids A **5**, 2600–2609 (1993).

[71] M. R. Jovanović and B. Bamieh, "Frequency domain analysis of the linearized Navier-Stokes equations," in *Proc. American Control Conference* (Denver, CO, 2003) pp. 3190–3195.

[72] B. Bamieh and M. Dahleh, "Energy amplification in channel flows with stochastic excitation," Phys. Fluids **13**, 3258–3269 (2001).

[73] This operator is a function of the wall-normal extent $y$.

[74] M. Jovanović and B. Bamieh, "Componentwise energy amplification in channel flows," J. Fluid Mech. **534**, 145–183 (2005).

[75] M. R. Jovanović and B. Bamieh, "Unstable modes versus non-normal modes in supercritical channel flows," in *Proceedings of the* 2004 *American Control Conference* (Boston, MA, 2004) pp. 2245–2250.

[76] B. J. McKeon and A. S. Sharma, "A critical-layer framework for turbulent pipe flow," J. Fluid Mech. **658**, 336–382 (2010).

[77] B. J. McKeon, A. S. Sharma, and I. Jacobi, "Experimental manipulation of wall turbulence: a systems approach," Phys. Fluids **25**, 031301 (2013).

[78] P. J. Schmid, "Nonmodal stability theory," Annual Rev. Fluid Mech. **39**, 129–162 (2007).

[79] A. S. Sharma and B. J. McKeon, "On coherent structure in wall turbulence," J. Fluid Mech **728**, 196–238 (2013).

[80] R. Moarref, A. S. Sharma, J. A. Tropp, and B. J. McKeon, "Model-based scaling of the streamwise energy density in high-Reynolds-number turbulent channels," J. Fluid Mech. **734**, 275–316 (2013).

[81] R. Moarref, M. R. Jovanović, J. A. Tropp, A. S. Sharma, and B. J. McKeon, "A low-order decomposition of turbulent channel flow via resolvent analysis and convex optimization," Phys. Fluids **26**, 051701 (2014).

[82] A. S. Sharma, R. Moarref, and B. J. McKeon, "Scaling and interaction of self-similar modes in models of high reynolds number wall turbulence," Philos. Trans. Roy. Soc. London A **375**, 20160089 (2017), https://royalsocietypublishing.org/doi/pdf/10.1098/rsta.2016.0089.

[83] T. DelSole, "Can quasigeostrophic turbulence be modeled stochastically?" J. Atmospheric Sciences **53**, 1617–1633 (1996).

[84] S. M. Tobias and J. B. Marston, "Direct statistical simulation of out-of-equilibrium jets," Phys. Rev. Lett. **110**, 104502 (2013).

[85] J. B. Marston, "Statistics of the general circulation from cumulant expansions," Chaos **20**, 041107 (2010).

[86] K. Srinivasan and W. R. Young, "Zonostrophic instability," J. Atmospheric Sciences **69**, 1633–1656 (2012).

[87] M-A. Nikolaidis, B. F. Farrell, and P. J. Ioannou, "The mechanism by which nonlinearity sustains turbulence in plane Couette flow," Journal of Physics: Conference Series **1001**, 012014 (2018).

[88] B. F. Farrell and P. J. Ioannou, "Statistical state dynamics-based analysis of the physical mechanisms sustaining and regulating turbulence in Couette flow," Phys. Rev. Fluids **2**, 084608 (2017).

[89] B. F. Farrell and P. J. Ioannou, "A theory of baroclinic turbulence," J. Atmospheric Sciences

**66**, 2444–2454 (2009).

[90] F. Ait-Chaalal, T. Schneider, B. Meyer, and J. B. Marston, "Cumulant expansions for atmospheric flows," New J. Phys. **18**, 025019 (2016).

[91] J. B. Marston, G. P. Chini, and S. M. Tobias, "Generalized quasilinear approximation: Application to zonal jets," Phys. Rev. Lett. **116**, 214501 (2016).

[92] A. Child, R. Hollerbach, B. Marston, and S. Tobias, "Generalised quasilinear approximation of the helical magnetorotational instability," J. Plasma Phys. **82**, 905820302 (2016).

[93] S. M. Tobias and J. B. Marston, "Three-dimensional rotating couette flow via the generalised quasilinear approximation," J. Fluid Mech. **810**, 412–428 (2017).

[94] D. F. Gayme, B. J. McKeon, A. Papachristodoulou, B. Bamieh, and J. C. Doyle, "A streamwise constant model of turbulence in plane Couette flow," J. Fluid Mech. **665**, 99–119 (2010).

[95] J-L. Bourguignon and B. J. McKeon, "A streamwise-constant model of turbulent pipe flow," Phys. Fluids **23**, 095111 (2011).

[96] K. M. Bobba, *Robust Flow Stability: Theory, Computations and Experiments in Near Wall Turbulence*, Ph.D. thesis, California Institute of Technology, Pasadena, CA, USA (2004).

[97] A. Papachristodoulou, *Scalable Analysis of Nonlinear Systems Using Convex Optimization*, Ph.D. thesis, California Institute of Technology, Pasadena, USA (2005).

[98] V. Thomas, B. Farrell, P. Ioannou, and D. F Gayme, "A minimal model of self-sustaining turbulence," Phys. Fluids **27**, 105104 (2015).

[99] J. U. Bretheim, C. Meneveau, and D. F. Gayme, "Standard logarithmic mean velocity distribution in a band-limited restricted nonlinear model of turbulent flow in a half-channel," Phys. Fluids **27**, 011702 (2015).

[100] B. A. Minnick and D. F. Gayme, "Characterizing energy transfer in restricted nonlinear wall-bounded turbulence," in *International Symposium on Turbulence and Shear Flow Phenomena (TSFP-11)* (2019).

[101] J. Jiménez, "Cascades in wall-bounded turbulence," Ann. Rev. Fluid Mech. **44**, 27–45 (2012).

[102] J. Gorski, J. M. Wallace, and P. S. Bernard, "The enstrophy equation budget of bounded turbulent shear flows," Phys. Fluids **6**, 3197 (1994).

[103] B. F. Farrell, D. F. Gayme, P. Ioannou, B. Lieu, and M. Jovanović, "Dynamics of the roll and streak structure in transition and turbulence," in *Proc. of the Center for Turbulence Research Summer Program* (2012) pp. 34–54.

[104] B. F. Farrell and P. J. Ioannou, "Optimal excitation of three dimensional perturbations in viscous constant shear flow," Phys. Fluids **5**, 1390–1400 (1993).

[105] J. U. Bretheim, C. Meneveau, and D. F. Gayme, "A restricted nonlinear large eddy simulation model for high Reynolds number flows," Journal of Turbulence **19**, 141–166 (2018).

[106] S. B. Pope, "Turbulent flows," (Cambridge University Press, Cambridge, UK, 2000) 1st ed.

[107] B. F. Farrell and P. J. Ioannou, "Structure and spacing of jets in barotropic turbulence," J. Atmospheric Sciences **64**, 3652–3665 (2007).

[108] F. Alizard and D. Biau, "Restricted nonlinear model for high- and low-drag events in plane channel flow," J. Fluid Mech. **864**, 221–243 (2019).

[109] J. U. Bretheim, C. Meneveau, and D. F. Gayme, "The restricted nonlinear large eddy simulation approach to reduced-order wind farm modeling," J. Renewable and Sustainable Energy **10**, 043307 (2018).

[110] A. S. Sharma, R. Moarref, B. J. McKeon, J. S. Park, M. D. Graham, and A. P. Willis, "Low-dimensional representations of exact coherent states of the Navier-Stokes equations from the resolvent model of wall turbulence," Phys. Rev. E **93**, 021102 (2016).

[111] M. A. Ahmed and A. Sharma, "New equilibrium solution branches of plane Couette flow discovered using a project-then-search method," ArXiv e-prints (2017), arXiv:arXiv:1706.05312.

[112] F. Alizard, "Invariant solutions in a channel flow using a minimal restricted nonlinear model," Comptes Rendus Mécanique **345**, 117–124 (2017).

[113] M. Pausch, Q. Yang, Y. Hwang, and B. Eckhardt, "Quasilinear approximation for exact coherent states in parallel shear flows," Fluid Dyn. Res. **51**, 011402 (2019).